Title
Time-domain Green's function for an infinite sequentially excited periodic line array of dipoles

Journal
IEEE Transactions on Antennas and Propagation, 48(6)

ISSN
0018-926X

Authors
Felsen, LB
Capolino, F

Publication Date
2000-06-01

DOI
10.1109/8.865225

Time-Domain Green's Function for an Infinite Sequentially Excited Periodic Line Array of Dipoles

Leopold B. Felsen, *Life Fellow, IEEE* and Filippo Capolino, *Member, IEEE*

***Abstract*—Green's functions based on truncated periodicity play an important role in the efficient analysis of radiation from, or scattering by, phased-array antennas, frequency selective surfaces and related applications. Such Green's functions exploit the equivalence between summation over the contributions from individual elements in an array and their collective treatment via Poisson summation in terms of an infinite series of Floquet waves (FW). While numerous explorations have been carried out in the frequency domain (FD), much less has been done for transient excitation. In order to gain understanding of the FW critical parameters and phenomenologies governing time-domain (TD) periodicity, we consider the simple canonical problem of radiation from an infinite periodic line array of sequentially pulsed axial dipoles. This problem can be solved in closed form and also by a variety of alternative representations, which include inversion from the FD, spectral decomposition into TD plane waves, the complex space–time analytic signal formulation, and the Cagniard–de Hoop method. These alternatives, some of which apply traditionally only for nondispersive TD events, are shown to still work here because of the special character of the FW dispersion. Particular attention is given to evanescent TD-FW's and their transition through cutoff. Asymptotic techniques grant insight into the TD-FW behavior by identifying their instantaneous frequencies, wavenumbers, and other physics-based parameterizations. A basic question concerns the definition of what constitutes a physically "observable" (causal, etc.) TD-FW. The proposed answer is based on consistency among models arrived at by alternative routes.**

***Index Terms*—Periodic arrays, spectral analysis and synthesis, time-domain Green's functions.**

I. Introduction

PERIODIC arrays of radiating or scattering elements play an important role in phased-array antennas, frequency selective surfaces, and related applications. Performance of such structures has been well explored in the frequency domain (FD), but only recently have such studies been extended to the time domain (TD) [1]–[3] . We have begun a systematic investigation of the TD behavior of dipole-excited Green's functions that are relevant for the characterization of truncated planar periodic arrays, with emphasis on the TD Floquet waves (FW) in the propagating *and* evanescent parameter regimes. Such waves on semi-infinite and finite rectangular arrays of dipoles have been and are being studied in the FD [4]–[7] and furnish the models for the explorations in the TD. The truncated array Green's functions lead to efficient parameterization of realistic arrays with slot elements, as demonstrated in [8] and [9]. Our initial aim is to understand the dispersive TD wave physics on simple canonical geometries, utilizing various methods that synthesize the solution from different perspectives. This paper deals with the first such configuration, an infinite periodic array of axial dipole radiators arranged along the z-axis of a rectangular or cylindrical coordinate system (Fig. 1), excited impulsively with interelement delay. The rules learned from this canonical problem will impact subsequent studies of phased line dipole array truncations and of rectangular truncated arrays with different longitudinal and transverse periodicities as well as different interelement phasings. The prototype problem is simple enough to admit of closed form exact solutions, which can be obtained via alternative routes as outlined in the Abstract. The phenomenologies associated with the driven dipole arrays are also relevant for oblique *plane wave scattering* by corresponding arrays of short wire elements, with the interelement phasing (time delay) determined by the obliquity, with respect to the array plane, of the incident field.

The problem to be studied is defined in Section II and is expressed there in terms of the FD and TD radiation from the individual dipole elements (local formulation). Alternatively the total wavefields can be expressed in terms of the periodicity-induced Floquet waves (global formulation). For better understanding of the basic wave physics, we retain simultaneous awareness of the local–global alternatives, which are quantified by the Poisson summation formulas in Section III. In Section IV, in the FD, we demonstrate the equivalence between the infinite sum of n-indexed linearly phased dipole-radiated fields and an infinite sum of q-indexed equivalent globally restructured Floquet wave fields FW_q radiated by *smoothly* phased FW line sources. The exact closed form results are examined asymptotically, with ray interpretations in the propagating FW (PFW) and evanescent FW (EFW) regimes. In Section V, we deal with the TD-FW. Performing conventional Fourier inversion from the FD in Section V-A yields a set of closed-form space–time-dependent Floquet waves. The

Manuscript received February 5, 1999; revised March 17, 2000. The work of L. B. Felsen was supported in part by the U.S.-Israel Binational Science Foundation, Jerusalem, Israel, under Grant 95-00399, and by ODDR&E under MURI Grant ARO DAAG55-97-1-0013 and Grant AFOSR F49620-96-1-0028. The work of F. Capolino was supported by the Commission for Educational and Cultural Exchange between Italy and the U.S. under a Fulbright Grant awarded in 1997 to conduct research at Boston University, Boston, MA.

L. B. Felsen is with the Department of Aerospace and Mechanical Engineering and the Department of Electrical and Computer Engineering, Boston University, Boston, MA 02215 USA.

F. Capolino is with the Dipartimento di Ingegneria dell'Informazione, Universitá degli Studi di Siena, 53100 Siena, Italy.

Publisher Item Identifier S 0018-926X(00)05796-3.

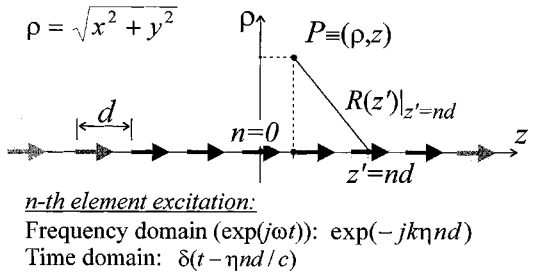

Fig. 1. Infinite periodic line array of electric current dipoles. Physical configuration, coordinates, and definitions: d = interelement spacing; $k = \omega/c$ = free space wavenumber; c = ambient wavespeed; $k\eta = \omega\gamma_z$ = interelement phasing; $\gamma_z = \eta/c = 1/v_z^{(p)}$ = interelement "slowness" (normalized wavenumber); $v_z^{(p)} = c/\eta$ = phase speed along z.

phenomenologies associated with these phased TD-FW$_q$ wave objects are investigated in detail and tied to physical models obeying causality, realvaluedness, etc., in fixed as well as moving coordinate frames. The TD-FW$_q$ are found to reveal a curiosity: though causal, they are complex. Pairing (summing) the $(+q)$ and $(-q)$ *complex* TD-FW's, however, generates a *real* wavefield. To explain this behavior, we have utilized in Section V-B the instantaneous FW$_q$ frequencies and spatial spectral wavenumbers k_q, which are related via the FW$_q$ dispersion relation $k_{zq} = \omega\eta/c + (2\pi q/d)$, $q = 0, \pm 1, \pm 2, \ldots$ where η/c and d are the interelement phase gradient and spacing, respectively. For different perspectives, in Sections V-C and V-D, we then treat the problem via the complex time, positive frequency only, *analytic signal* formulation [10]–[12] and via a generalization of the (nondispersive) Cagniard–de Hoop method [13], [14], respectively. For an individual TD-FW$_q$, each of the alternatives in Sections V-A–V-D addresses periodic phased-array phenomenology from a distinct vantage point. Each has its own nonphysical anomaly which can, however, be removed via $(+q)$, $(-q)$ pairing to produce the same unique causal physically observable wavefield. We believe the special role of the $(+q)$, $(-q)$ FW pair to be a new finding with relevance also for subsequent studies of truncated line and planar phased arrays. Conclusions are presented in Section VI.

II. Statement of the Problem

The geometry of the linear array of dipoles oriented along the z direction and excited by transient currents in free-space is shown in Fig. 1, with definition of both Cartesian and cylindrical coordinate systems. The period of the array is d. This simple array geometry generates a z-directed electric field E_z, from which all other field components can be derived. Moreover, the E_z field component is simply related to the z-directed magnetic scalar potential A, which shall be used throughout. The FD [$\exp(j\omega t)$ dependence] and TD potential fields are related by the Fourier transform pair

$$A(\boldsymbol{r}, \omega) = \int_{-\infty}^{\infty} \hat{A}(\boldsymbol{r}, t) e^{-j\omega t}\, dt,$$
$$\hat{A}(\boldsymbol{r}, t) = \frac{1}{2\pi} \int_{-\infty}^{\infty} A(\boldsymbol{r}, \omega) e^{j\omega t}\, d\omega \tag{1}$$

where a caret $\hat{}$ denotes a time-dependent function. Boldface symbols define vector quantities. It will be convenient to introduce the nondimensional parameter

$$\eta = c\gamma_z = c/v_z^{(p)} \tag{2}$$

which plays a fundamental role in the analysis. Here, $\gamma_z = 1/v_z^{(p)}$ denotes the interelement phase gradient and $v_z^{(p)}$ is the impressed phase speed along the array, which can be greater or smaller than the ambient propagation speed c.

The phased array FD and TD dipole currents $J(\omega)$ and $\hat{J}(t)$, respectively, are then related via (1) and are given by

$$\left.\begin{matrix} J(\omega) \\ \hat{J}(t) \end{matrix}\right\} = \sum_{n=-\infty}^{\infty} \delta(z' - nd) \left\{ \begin{matrix} e^{-jk\eta nd} \\ \delta(t - \eta nd/c) \end{matrix} \right\}, \qquad k = \frac{\omega}{c} \tag{3}$$

where k is the ambient wavenumber. In the n-dependent element current amplitudes multiplying the delta function in (3), the FD portion $k\eta d$ accounts for an assumed (linear) phase difference between adjacent elements. The TD portion identifies sequentially pulsed dipole elements, with the element at $z' = nd$ turned on at time $t_n = \eta nd/c$.

III. Poisson Summation

The Poisson sum formula is given in its most elementary form by $\sum_{n=-\infty}^{\infty} \delta(z' - nd) = d^{-1} \sum_{q=-\infty}^{\infty} \exp(-j2\pi q z'/d)$ [15, pp. 117] and it becomes for the infinite series of phased n-indexed FD and TD elements in (3)

$$\sum_{n=-\infty}^{\infty} \left\{ \begin{matrix} e^{-jk\eta nd} \\ \delta(t - \eta nd/c) \end{matrix} \right\} \delta(z' - nd) = \frac{1}{d} \sum_{q=-\infty}^{\infty} \left\{ \begin{matrix} e^{-jk_{zq} z'} \\ e^{-j\alpha_q z'} \delta(t - \eta z'/c) \end{matrix} \right. \tag{4}$$

where $k_{zq}(\omega)$ represents a Floquet-type dispersion relation

$$k_{zq}(\omega) = k\eta + \alpha_q, \qquad \alpha_q = \frac{2\pi q}{d},\ q = 0, \pm 1, \pm 2, \cdots. \tag{5}$$

Thus, in the FD, Poisson summation converts the effect of the infinite periodic array of *individual phased* n-indexed *dipole* radiators collectively into an infinite superposition of linearly *smoothly phased* q-indexed equivalent *line source* distributions along the axis of the dipole array. The equivalent smoothly phased-line sources furnish the initial conditions that characterize propagating and evanescent Floquet-type wave behavior, which we shall refer to as PFW and EFW, respectively. In the TD, the n-indexed sequentially pulsed dipoles are converted collectively into smoothly phased, q-indexed impulsive source distributions that travel with the phase speed $v_z^{(p)} = c/\eta$ so that their location at z' corresponds to the time $t_{z'} = \eta z'/c$. This suggests referencing time to a moving coordinate frame via $\tau(z) = t - \eta z/c$.

IV. Floquet Waves: Frequency Domain

To obtain for the potential fields $A_n(\boldsymbol{r}, \omega)$ radiated by the linearly phased dipole array element currents an equivalent sum

of FW potentials $A_q^{\rm FW}(\boldsymbol{r}, \omega)$ radiated by the smoothly phased FW-modulated line sources, we multiply the FD portion of (4) by the FD element Green's function

$$A(\boldsymbol{r}, z', \omega) = \frac{e^{-jkR(z')}}{4\pi R(z')}$$
$$R(z') = \sqrt{\rho^2 + (z - z')^2} \tag{6}$$

and perform the integration $\int_{-\infty}^{\infty} dz'$ to generate $A_n = A(\boldsymbol{r}, nd, \omega)\exp(-jk\eta nd)$, with $\boldsymbol{r} = (\rho, z)$, on the left side of (4). On the right side of (4), this yields the collective FW-phased line source Green's functions

$$A_q^{\rm FW}(\boldsymbol{r}, \omega) = \frac{1}{d}\int_{-\infty}^{\infty} \frac{e^{-jkR(z')}}{4\pi R(z')}\, e^{-jk_{zq}z'}\, dz'$$
$$= \frac{e^{-jk_{zq}z}}{4jd}\, H_0^{(2)}(k_{\rho q}\rho). \tag{7}$$

The closed-form result in (7) follows from a known Fourier transform [16, pp. 493]. The radial FW$_q$ wavenumber $k_{\rho q}$ is given in terms of the z-domain wavenumber k_{zq} by

$$k_{\rho q}(\omega) = \sqrt{k^2 - k_{zq}^2}, \qquad k = \omega/c. \tag{8}$$

The square-root function in (8) is defined so that $\Im m k_{\rho q} \leq 0$ on the top Riemann sheet, consistent with the radiation condition at $\rho = \infty$. Furthermore, $\Re e k_{\rho q} \geq 0$ or ≤ 0 for $\omega > 0$ or < 0, respectively, in order to satisfy the radiation condition for positive and negative real frequencies (see Appendix B for more details).

In (7), Floquet waves with z-domain propagation constants $|k_{zq}| < |k|$ characterize radially propagating FW's (PFW), while those with $|k_{zq}| > |k|$ characterize radially evanescent FW's (EFW). This follows from the properties of the Hankel function in (7). Using the asymptotic approximation $H_0^{(2)}(k_{\rho q}\rho) \sim \sqrt{2/(\pi k_{\rho q}\rho)}\, \exp(j(\pi/4 - k_{\rho q}\rho))$ leads to

$$A_q^{\rm FW}(\boldsymbol{r}, \omega) \sim \frac{e^{-j\pi/4}\sqrt{2}}{4d\sqrt{\pi k_{\rho q}\rho}}\, e^{-j(k_{\rho q}\rho + k_{zq}z)}. \tag{9}$$

The phase term can be written as $\exp(-j\boldsymbol{k}_q^{\rm FW}\cdot\boldsymbol{r})$, with $\boldsymbol{r} = \rho\boldsymbol{i}_\rho + z\boldsymbol{i}_z$ denoting the position vector, $\boldsymbol{i}_\rho$ and $\boldsymbol{i}_z$ denoting unit vectors along ρ and z, respectively, and $\boldsymbol{k}_q^{\rm FW} = k_{\rho q}\boldsymbol{i}_\rho + k_{zq}\boldsymbol{i}_z$ denoting the total FW$_q$ propagation vector. The propagating characteristics of the PFW and EFW for positive and negative frequencies are schematized in Fig. 2. By phase matching along z, each PFW contributes at the observation point $\boldsymbol{r} \equiv (\rho, z)$ a ray asymptotic field originating at a point $\overline{z}_q'$ on the z-axis. The rays emanating from the point $\overline{z}_q'$ lie on the ray cone with semi-angle

$$\beta_q = \cos^{-1}(k_{zq}/k) \tag{10}$$

which definition applies to positive or negative frequencies. It then follows from (5) and (10), as shown in Fig. 2(a), that for $q \neq 0$, $\omega > 0$ and $\omega < 0$ give rise to two different FW$_q$ propagation angles. When k_{zq} approaches $\pm k$, the cone angle β_q tends to zero or π, respectively. Beyond that limit, when $|k_{zq}| > |k|$, the cone angle becomes complex and the field becomes evanescent along ρ. The condition $|k_{zq}| = |k|$, i.e., $k_{\rho q} = 0$, is the cutoff condition for the qth FW where the propagating-to-evanescent transition occurs [4], [5] for both $\omega \gtrless 0$ [cf. (29)]. Owing to the exponential attenuation of EFW$_q$ along ρ, the EFW portion of $\sum_{q=-\infty}^{\infty} A_q^{\rm FW}$ converges rapidly away from the array axis and a few terms may suffice for an adequate approximation of the total radiated field.

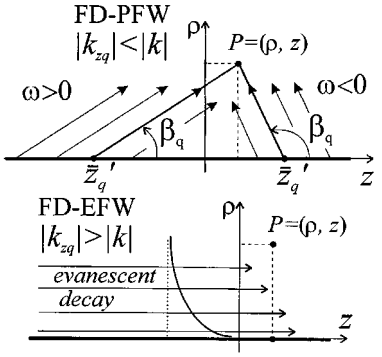

Fig. 2. FD qth Floquet-type equivalent continuous line source distributions. (a) $|k_{zq}| < |k|$. (b) $|k_{zq}| > |k|$. The FD FW$_q$ rays are parallel, with direction determined by $k_{zq} = k\ \sin\ \beta_q$. The ray to the observer originates at $\overline{z}_{q,\pm}'$ for positive and negative frequencies. The radiation angle β_q, $q = \pm 1, \pm 2, \ldots$ [see (10)] is different, while β_0 is the same for positive and negative frequencies. In (b), when $|k_{zq}| > |k|$, the field is evanescent along the ρ-direction.

V. Floquet Waves: Time Domain

A. Direct Inversion from the Frequency Domain

Since the FD-n series has summands $A_n = A(\boldsymbol{r}, nd, \omega)\exp(-j\omega\eta nd/c)$ composed of two ω-dependent functions [see text after (6)], the TD $\hat{A}_n(\boldsymbol{r}, t)$ involves a convolution. First, from (6) and (1), one finds that $\hat{A}(\boldsymbol{r}, z', t) = \delta(t - R(z')/c)/(4\pi R(z'))$. When this function is time-convolved with the TD portion on the left side of (4), i.e., $\int_{-\infty}^{\infty} dt' A(\boldsymbol{r}, z', t - t')\delta(t' - \eta nd/c)$, followed by $\int_{-\infty}^{\infty} dz'$, one obtains the field $\hat{A}_n(\boldsymbol{r}, t)$ excited by the impulsive nth dipole current in (3)

$$\hat{A}_n(\boldsymbol{r}, t) = \frac{\delta(t - \eta nd/c - R(nd)/c)}{4\pi R(nd)} \tag{11}$$

which represents a spherical impulsive wavefront radiated by the dipole at $z' = nd$, with $R(z')$ taken from (6). The same operations applied to the right-hand side of (4) or direct FD inversion of (7) yields the TD-FW

$$\hat{A}_q^{\rm FW}(\boldsymbol{r}, t) = \frac{1}{4\pi d}\int_{-\infty}^{\infty} \frac{e^{-j\alpha_q z'}}{R(z')}\, \delta\left(t - \frac{\eta z'}{c} - \frac{R(z')}{c}\right) dz'. \tag{12}$$

The argument of the delta function in (12) identifies the integral as a Radon slant-stack projection transform [17] (normalized to the unit cell width d). The integrand in (12) contributes only for those real z'-values in Appendix A which satisfy, in the moving coordinate frame

$$\tau + \frac{\eta(z - z')}{c} - \frac{R(z')}{c} = 0, \qquad \tau = t - \eta z/c. \tag{13}$$

The radiating case is described by $|\eta| < 1$, the nonradiating case by $|\eta| > 1$ and the transition between the two by $|\eta| = 1$. The

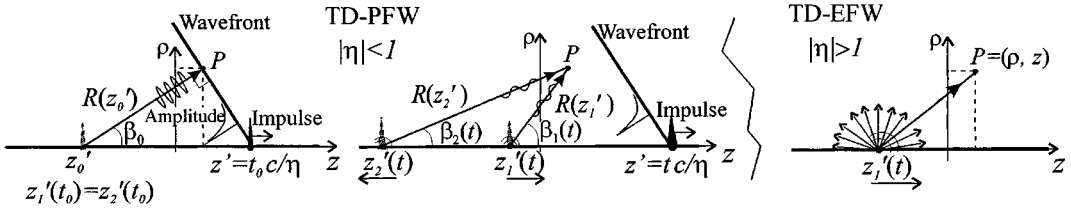

Fig. 3. TD qth Floquet-type equivalent continuous line source distribution. (a), (b) (Radiating) $|\eta| < 1$. (c) (Nonradiating) $|\eta| > 1$. (a) At turn-on $t = t_0(\rho,\ z)$, all TD-FW$_q$ arrive from a direction β_0 independent of q and the current impulse is located at $z' = t_0 c/\eta$. The first signal arrival at the observer originates at the earlier point z_0'. (b) For $t > t_0$ $z_1'(t)$, and $z_2'(t)$ are the two real (propagating) solutions of the TD-FW dispersion equation (13). Two distinct contributions arrive at the observer simultaneously from the q-independent directions $\beta_1(t)$ and $\beta_2(t)$. (c) One real solution of (13): $z_1'(t)$ when $\eta > 0$ or $z_2'(t)$ when $\eta < 0$ for all t. Field at the observer at time t originates from the point $z_1'(t)$ when $\eta > 0$.

"nonradiating" case is characterized by the absence of a wavefront (i.e., turn-on time) and is discussed further in Sections V-A and V-B.We now explore the various solutions that can be associated with the FW index $|q|$.

1) Radiating Case: $|\eta| < 1$: Fundamental solution. For the radiating case $|\eta| < 1$, with $\tau > 0$, (13) has the two solutions $z_1'(t)$ and $z_2'(t)$ (see Appendix A)

$$z_i'(t) = z - \frac{c}{1-\eta^2}\left(\tau\eta + (-1)^i\sqrt{\tau^2 - \tau_0^2}\right), \qquad i = 1,\ 2 \tag{14}$$

on the top sheet of the complex z' plane defined by $\Re e R(z') > 0$ (Fig. 6). In (14)

$$\tau_0 \equiv \sqrt{1-\eta^2}\rho/c = t_0 - \eta z/c \tag{15}$$

where (13) is used for the second equality in (15). Here, $\Re e\sqrt{1-\eta^2} \geq 0$ and $\Im m\sqrt{1-\eta^2} \leq 0$; this is in accord with (8) since $\sqrt{k^2(1-\eta^2)} = k_{\rho q}|_{q=0}$. Note that $z_i'(t)$ does *not depend on* q; moreover, $z_i'(t) - z = \text{const.}$ in the moving coordinate frame $\tau = \text{const.}$ The two real solutions of (13) for $\tau > \tau_0$ (i.e., $t > t_0$) coincide at $\tau = \tau_0$ (i.e., $t = t_0$), which represents the causal turn-on time $t_0 = \eta z/c + \sqrt{1-\eta^2}\rho/c$ with launch point $z_0' = z_1'(t_0) = z_2'(t_0)$, as in Fig. 3(a); $\tau_0 = \sqrt{1-\eta^2}\rho/c$ is the causal turn-on time when the wavefront arrives at the observer. In the moving coordinate system, τ_0 represents the wavefront arrival delay that the moving observer encounters with respect to the exciting impulse current located at $z' = tc/\eta$ [Fig. 3(a) and (b)]. The point z_0' coincides with $\overline{z}_0'$ in Fig. 2 (not shown), from which the $q = 0$ FD-FW is launched toward the observer. For $t > t_0$, these solutions separate according to (14) and move toward $z_1'(t) \to +\infty$ and $z_2'(t) \to -\infty$ Fig. 3(b). For $\tau < \tau_0$, i.e., $t < t_0$, the two solutions are conjugate complex and do not lie on the integration path; thus the integral in (12) vanishes for $\tau < \tau_0$ (causality). The two *causal* field contributions corresponding to $z_1'(t)$ and $z_2'(t)$ are determined by recalling that $\delta[f(z')] = \delta(z - z_i')|df/dz'|^{-1}_{z_i'}$ when $f(z_i') = 0$. Substituting for $R(z_i'(t))$ from (13) and (14) and simplifying, one obtains what we shall refer to as the causal *fundamental solution* for the $(q,\ i)$ indexed TD-FW,

$$\hat{A}^{\text{PFW}}_{q,\,i}(\boldsymbol{r},\ t) = \frac{e^{-j\alpha_q z_i'(t)}}{4\pi d\sqrt{\tau^2 - \tau_0^2}}\,U(\tau - \tau_0), \qquad i = 1,\ 2 \tag{16}$$

where $\boldsymbol{r} = (\rho,\ z)$, and $U(\tau - \tau_0) \equiv U(t - t_0)$, with $U(\tau) = 1$ or 0 if $\tau > 0$ or $\tau < 0$, respectively. The physical interpretation of the result in (16) follows. First, in the moving coordinate frame, each $\hat{A}^{\text{PFW}}_{q,\,i} = \text{const.}$ since $\tau = \text{const.}$ and $z_i'(t) = \text{const.}$ there. However, for a stationary observer at P, each of the $i = 1$ or $i = 2$ PFW contributions in (16) is shown in Fig. 3(a) and (b). Although the $i = 1$ and $i = 2$ TD-FW$_q$ waves are distinct, we treat them together in Fig. 3(a) and (b) to contrast their individual behavior. At the turn-on time $\tau = \tau_0$, when the wavefront reaches P in Fig. 3(a), the current impulse is located at $z' = t_0 c/\eta = t_0 v_z^{(p)}$, where the wavefront originates. At the earlier time $t' = t - R(z_0')/c$, the current impulse was located at the point z_0', and $R(z_0')/c$ is the time required for the field launched from z_0' to reach the observer. The angle β_0 is here defined as $\cos\beta_0 = (z - z_0')/R(z_0')$ and coincides with that in (10) for $q = 0$ (i.e., $\alpha_q = 0$). This implies that at the turn-on time t_0 pertaining to the fixed observation point P, the wavefront arrives from a direction coincident with that of the FD-FW wave vector $\boldsymbol{k}_0^{\text{FW}}$ in the text after (9).

At times $\tau > \tau_0$, the wavefront moves beyond P to the location shown in Fig. 3(b), which is tagged on the z axis by $z' = tc/\eta = tv_z^{(p)}$. The observer now receives two distinct contributions that arrive simultaneously but are launched from points $z_i'(t)$, $i = 1,\ 2$ at times $t_i' = t - R(z_i'(t))/c$, respectively, in accord with the moving current impulse on the right side of (4). The two angles $\beta_i(t)$ depicted in Fig. 3(b) defined as

$$\cos\beta_i = (z - z_i'(t))/R(z_i'(t)), \qquad i = 1,\ 2 \tag{17}$$

are given explicitly via substitution from (13) and (14) by

$$\cos\beta_i(t) = \frac{(-1)^i\,\sin^2\beta_0\sqrt{1 - \left(\frac{\tau_0}{\tau}\right)^2} + \cos\beta_0\left(\frac{\tau_0}{\tau}\right)^2}{\sin^2\beta_0 + \cos^2\beta_0\left(\frac{\tau_0}{\tau}\right)^2} \tag{18}$$

where $i = 1,\ 2$ and $\beta_0 = \cos^{-1}(\eta)$. For the $q = 0$ mode ($\alpha_q = 0$), $\hat{A}_0^{\text{PFW}} = \hat{A}_{0,1}^{\text{PFW}} + \hat{A}_{0,2}^{\text{PFW}}$ in (16) agrees exactly with the real field radiated by an impulsively excited smooth infinite line source with axial phasing specified by η/c [16, pp. 495]. The result in (16) represents the most elementary form of the qth TD Floquet wave parameterized by its point of emergence $z_i'(t)$, $i = 1,\ 2$, on the array. Although obtained by conventional Fourier inversion from the FD, for $|q| > 0$ ($\alpha_q \neq 0$), the result in (16) is complex. This behavior can be attributed to the fact that the FD-FW $A_q^{\text{FW}}(\boldsymbol{r},\ \omega)$ in (7) does not satisfy the relation $A_q^{\text{FW}}(\boldsymbol{r},\ -\omega) = [A_q^{\text{FW}}(\boldsymbol{r},\ \omega)]^*$ (* denotes complex conjugate) which would guarantee a real TD function $\hat{A}_q^{\text{FW}}(\boldsymbol{r},\ t)$ (see

Appendix B). Furthermore, we note that also the instantaneous PFW$_{q,i}$ frequencies $\omega_{q,i}(t)$, defined by $(d/dt)[-\alpha_q z_i'(t)]$, are not such that the complex conjugate relation $Q(-\omega) = Q^*(\omega)$ is satisfied. Details are discussed in Section V-B, which is devoted to the asymptotic evaluation of the Fourier inversion integral in (1). To obtain a physical (i.e., real causal) field from (16), we take

$$\Re e\hat{A}_{q,i}^{\mathrm{PFW}}(\boldsymbol{r}, t) = \frac{\cos(\alpha_q z_i'(t))}{4\pi d\sqrt{\tau^2 - \tau_0^2}}\, U(\tau - \tau_0) \tag{19}$$

with $i = 1, 2$. The *fundamental* solution in (16), with (19), can be used to synthesize various combinations of $\hat{A}_{q,i}^{\mathrm{PFW}}$ fields which all contribute at the *same* instant t to the field at $\boldsymbol{r} = (\rho, z)$. Note that this solution is the same for $(+q)$ and $(-q)$ since $\alpha_{-q} = -\alpha_q$.

Combining $i = 1$ and $i = 2$. This gives

$$\Re e\hat{A}_{q}^{\mathrm{PFW}} \equiv \Re e\hat{A}_{q,1}^{\mathrm{PFW}} + \Re e\hat{A}_{q,2}^{\mathrm{PFW}}. \tag{20}$$

Combining $(+q)$ and $(-q)$. Adding the $(+q)$ and $(-q)$ contributions for $i = 1$ or 2 from (16) *directly* yields the *real* field

$$\hat{A}_{i}^{|q|\mathrm{PFW}} \equiv \hat{A}_{+q,i}^{\mathrm{PFW}} + \hat{A}_{-q,i}^{\mathrm{PFW}} = 2\Re e\hat{A}_{q,i}^{\mathrm{PFW}} \tag{21}$$

with $i = 1, 2$. This result implies that $(+q)$ and $(-q)$ pairing restores the positive–negative frequency relation obeyed by *conventional* Fourier synthesis, thereby assigning a special *physical significance* to the $(+q)$, $(-q)$ *sum* of complex TD-FW$_{q,i}$ (see Fig. 4) for *either* $i = 1$ or $i = 2$. To the best of our knowledge, this property has not been observed previously.

Combining $(\pm q)$ and $i = 1, 2$: the observable TD-FW$_q$. Since the $i = 1, 2$ superposition is independent of the sign of q, implementing the $(+q)$, $(-q)$ superposition in addition merely doubles the result in (20), i.e.,

$$\Re e\hat{A}^{|q|\mathrm{PFW}} = \Re e(\hat{A}_{q}^{\mathrm{PFW}} + \hat{A}_{-q}^{\mathrm{PFW}}) = 2\Re e\hat{A}_{q}^{\mathrm{PFW}}. \tag{22}$$

The same result is obtained when adding the $i = 1$ and $i = 2$ contributions in (21), using (19). In summary, $\Re e\hat{A}^{|q|\mathrm{PFW}} \equiv \hat{A}_{obs}^{|q|\mathrm{PFW}} = \hat{A}_{q}^{\mathrm{PFW}} + \hat{A}_{-q}^{\mathrm{PFW}} = \hat{A}_{1}^{|q|\mathrm{PFW}} + \hat{A}_{2}^{|q|\mathrm{PFW}}$ with

$$\hat{A}_{obs}^{|q|\mathrm{PFW}} = \frac{\cos(\alpha_q z_1'(t)) + \cos(\alpha_q z_2'(t))}{2\pi d\sqrt{\tau^2 - \tau_0^2}}\, U(\tau - \tau_0). \tag{23}$$

The fact that the $(+q)$, $(-q)$ paired $\hat{A}_{obs}^{|q|\mathrm{PFW}} = \hat{A}_{q}^{\mathrm{PFW}} + \hat{A}_{-q}^{\mathrm{PFW}}$ is real is demonstrated *a priori* in Appendix B. There it is shown that FD $(+q)$, $(-q)$ pairing satisfies the relation $A_q^{\mathrm{FW}}(\boldsymbol{r}, -\omega) + A_{-q}^{\mathrm{FW}}(\boldsymbol{r}, -\omega) = [A_q^{\mathrm{FW}}(\boldsymbol{r}, \omega) + A_{-q}^{\mathrm{FW}}(\boldsymbol{r}, \omega)]^*$, which guarantees a real TD function $\hat{A}_{q}^{\mathrm{PFW}} + \hat{A}_{-q}^{\mathrm{PFW}}$.

We regard $\hat{A}_{obs}^{|q|\mathrm{PFW}}$ as the *observable field* associated with the $|q|$th TD-FW at the location $\boldsymbol{r} = (\rho, z)$ at the instant t. It is synthesized by the four $(\pm q)$, $i = 1, 2$, fundamental contributions, all of which arrive *simultaneously* at the stationary observer. This observable field turns out to be consistent with the one derived in (45) via the analytic signal formulation which restricts the (real) frequencies to $\omega > 0$ only, with time extended into the complex domain. As shown in (45), the result in (22), (23) is the *only one* that agrees with the causal field extracted via analytic signals. Since the analytic signal algorithm applies

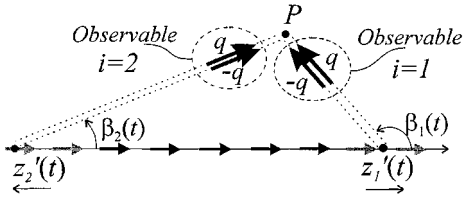

Fig. 4. Physical TD-FW observables synthesized by $(+q)$ and $(-q)$ pairing (radiating case $|\eta| < 1$). Each arrow also represents the group velocity vector $\boldsymbol{v}_{zq,\,i}^{(g)}$ of the pulsed $(q,\ i)$ wavefield, which arrives from different q-independent directions $\beta_i(t)$ for $i = 1$ and $i = 2$, respectively.

in general to wavefields with complex spectra, the above designation of (23) or (45) as the observable field is persuasive. The asymptotic instantaneous wavenumbers and frequencies, which parameterize the *fundamental* $\hat{A}_{q,i}^{\mathrm{PFW}}$ wavefield in (16) are identified in Section V-B (for instantaneous wavenumber and frequency extraction by TD wave processing, see [18]).

2) Nonradiating Case: $|\eta| > 1$: For the nonradiating case $|\eta| > 1$ we have from (15) that $\sqrt{1-\eta^2} = -j\sqrt{\eta^2 - 1}$ and thus $\tau_0 = -j|\tau_0|$. Now, as shown in Appendix A, (13) has only a single real solution $z_i'(t)$, which is valid for $\tau > 0$ and $\tau < 0$ provided that $i = 1$ for $\eta > 0$ and $i = 2$ for $\eta < 0$. Thus, the EFW solution corresponding to (16) is

$$\hat{A}_{q}^{\mathrm{EFW}}(\boldsymbol{r}, t) = \frac{e^{-j\alpha_q z_i'(t)}}{4\pi d\sqrt{\tau^2 + |\tau_0|^2}}, \qquad i = \begin{cases} 1, & \eta > 0 \\ 2, & \eta < 0 \end{cases} \tag{24}$$

for all τ. This evanescent FW field exists in all of space at all times and there is no wavefront [see Fig. 3(c)]. The result in (24) is complex. To obtain the physical (i.e., real) field from (24), we take the $\Re e\hat{A}_{q}^{\mathrm{EFW}} = \cos(\alpha_q z_i'(t))/[4\pi d(\tau^2 + |\tau_0|^2)^{1/2}]$, which is valid for both $(+q)$ and $(-q)$. Adding the $(+q)$ and $(-q)$ contributions *directly* from (24) yields a *real* field

$$\hat{A}^{|q|\mathrm{EFW}} \equiv \hat{A}_{q}^{\mathrm{EFW}} + \hat{A}_{-q}^{\mathrm{EFW}} = 2\Re e\hat{A}_{q}^{\mathrm{EFW}}, \qquad |q| > 0. \tag{25}$$

This result implies that $(+q)$ and $(-q)$ pairing restores the positive–negative frequency relation obeyed by the conventional Fourier synthesis not only for the radiating case (see Appendix B) but also for the evanescent case. Both the radiating and evanescent regimes are accommodated together by the analytic signal formulation in Section V-C.

3) Moving Particle Analogy: The results in (20) and (24) have an interesting physical interpretation based on wavefield solutions generated by a moving particle. For the FW with $q = 0$, both the radiating and nonradiating wavefields in (20) and (24) are identical with the fields produced by a static point charge moving with speed $v > c/\sqrt{\epsilon_r}$ and $v < c/\sqrt{\epsilon_r}$, respectively, inside a nondispersive dielectric medium with relative permittivity ϵ_r provided that v is replaced by $v_z^{(p)}$ and the normalization factor $1/d$ is included [16, pp. 495]. The parameter regimes $v > c/\sqrt{\epsilon_r}$ and $v < c/\sqrt{\epsilon_r}$ correspond to supersonic and subsonic motion, respectively, with respect to the ambient medium. The former leads to a causal progressive conical wavefront disturbance perpendicular to rays with wavevector $\boldsymbol{k}_0^{\mathrm{FW}}$, which defines the ray cone β_0 in (10); the latter yields a quasi-static field which occupies all of space at all times, as schematized in Fig. 3(c). In the FW analog, the supersonic or subsonic speeds in vacuum are those of the

coordinate frame moving with the periodicity-induced phase speed $v_z^{(p)} = c/\eta$. For $q \neq 0$, the moving source carries with it a phase given by the numerators in (16) and (24) for the supersonic and subsonic cases, respectively. This phase produces the dynamic modulations associated with the moving center along the z-axis ($\tau(z) = t - \eta z/c$), which appears in the TD observables in (23) and in (25).

B. Asymptotics

1) Local Frequencies and Wavenumbers: Additional information about the $\hat{A}_q^{\mathrm{FW}}(\boldsymbol{r}, t)$ behavior can be extracted from the high-frequency asymptotic evaluation of the $\hat{A}_q^{\mathrm{FW}}(\boldsymbol{r}, t)$ inversion integral in (1), using the asymptotic approximation (9) for the FW in order to extract the instantaneous frequency and wavenumber dependence

$$\hat{A}_q^{\mathrm{FW}}(\boldsymbol{r}, t) \sim \int_{-\infty}^{\infty} F(\omega) e^{-j\hat{\psi}(\omega)}\, d\omega \tag{26}$$

where $F(\omega) = \exp(-j\pi/4)(8\pi d)^{-1}\sqrt{2/(\pi k_{\rho q}\rho)}$ accounts for the slowly varying amplitude terms in the integrand and the phase is

$$\hat{\psi}(\omega) = k_{zq} z + k_{\rho q}\rho - \omega t \tag{27}$$

with $k_{zq}(\omega)$ and $k_{\rho q}(\omega)$ given in (5) and (8), respectively. The dominant contributions to the integral in the high-frequency range arise from the stationary (saddle) points ω_q of $\hat{\psi}(\omega)$, defined by $(d\hat{\psi}/d\omega)|_{\omega_q} = 0$. For $q = 0$, the FW is nondispersive and is therefore not reduceable by saddle-point approximation since $d\hat{\psi}/d\omega$ is then ω independent. In the radiating case ($|\eta| < 1$), for $q \neq 0$, the real solutions yield (see Appendix C)

$$\omega_{q,i}(\boldsymbol{r}, t) = \frac{\alpha_q c}{1-\eta^2}\left(\eta + \frac{(-1)^i \tau}{\sqrt{\tau^2 - \tau_0^2}}\right), \quad i = 1, 2,\ \tau > \tau_0 \tag{28}$$

with τ and τ_0 defined in (13) and (15), respectively. The same expression can also be derived independently from the time dependent phase in (16) by performing the operation $\omega_{q,i}(t) = (d/dt)[-\alpha_q z_i'(t)]$. The two solutions in (28) represent *local instantaneous* frequencies of oscillation of the TD PFW$_q$ at a given point $\boldsymbol{r}$ and a given instant t. The $\omega_{q,i}$ are real in the causal domain $\tau > \tau_0$, they increase with mode index q but decrease with time t and approach their cutoff frequency when $\tau \to \infty$

$$\omega_{q,i}(t \to \infty) = \omega_{q,i}^{\mathrm{cutoff}} = \frac{\alpha_q c}{(-1)^i - \eta}, \qquad i = 1, 2. \tag{29}$$

The cutoff frequencies ($i = 1, 2$), which satisfy the cutoff condition $|k_{zq}| = |k|$ [see (10)], are independent of the location of the observer.

To illustrate the behavior of the local instantaneous oscillation frequencies in (28), we present a specific example. Fig. 5 shows a plot of the frequencies $f_{q,i} = \omega_{q,i}/(2\pi)$ for $q = 1, \ldots 8$ and $i = 1, 2$ in the range $(-2, +2)$ GHz versus the moving-center time reference $\tau = t - \eta z/c$. The array spacing is $d = 1$ m and the observer is located at the radial distance $\rho = 1$ m from the array. The pointing angle $\beta_0 = 60°$ corresponds to $\eta = 1/2$. One observes that the frequency of each PFW$_q$ ($i = 1, 2$) is

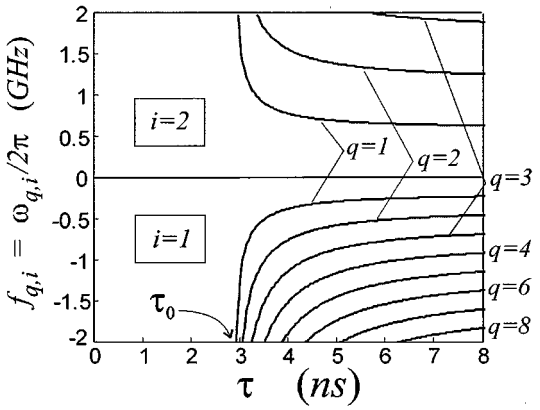

Fig. 5. Local frequencies of oscillation $f_{q,i} = \omega_{q,i}/(2\pi)$ of the TD-FW's versus $\tau = t - \eta z/c$. At turn-on $\tau = \tau_0$ ($t = t_0$), $f_{q,i} \to \infty$ for all q. The $f_{q,i}$ are real in the causal domain $\tau > \tau_0$, increase with mode index q, decrease with time τ and approach the q-dependent cutoff frequency in (29) when $\tau \to \infty$. Only $f_{q,i}$ with positive q are shown; the $(-q)$ values are obtained by $f_{-q,i} = -f_{q,i}$.

infinite at the turn-on time $\tau = \tau_0$ and decreases for $\tau > \tau_0$. Frequencies for PFW$_q$ with negative q are obtained from (28) by the relation $\omega_{q,i} = -\omega_{-q,i}$. The asymmetry between positive and negative frequencies is due to the interelement phase gradient $\eta/c \neq 0$. In fact, $\eta = 0$ in (28) leads to $\omega_{q,1} = -\omega_{q,2}$ and thus to symmetric frequency constituents. This was the case treated in [2] and [3]. It is seen that for $\eta > 0$, FW with $i = 1$ are more densely packed than those with $i = 2$ (vice versa for $\eta < 0$). Accordingly, a band-limited pulsed signal will excite a larger number of radiating PFW$_{q,1}$ modes than PFW$_{q,2}$ modes when $\eta > 0$, but vice versa when $\eta < 0$. If η increases in the range $\eta < 1$, $(1 - \eta^2)$ decreases [see (15)] and, thus, from (28), the frequency interval between q-indexed $i = 2$ positive frequencies increases, while those with $i = 1$ do not change significantly. Near the transition $|\eta| = 1$ between the radiating and the nonradiating cases, we have $(1 - \eta^2) \to 0$ and, thus, $|\omega_{q,1}(t)|$ or $|\omega_{q,2}(t)| \to \infty$ for every q and t for $\eta \to -1$ or $\eta \to 1$, respectively. However, these are trends only since the asymptotics fails when $k_{\rho q}\rho \to 0$. For the nonradiating case $|\eta| > 1$ every TD-EFW is characterized by only one contribution in (24), corresponding to the single real solution of $(d\hat{\psi}/d\omega)|_{\omega_q} = 0$ (see Appendix C).

The instantaneous saddle point frequencies $\omega_{q,i}(t)$ characterize corresponding instantaneous wavenumbers pertaining to the observer located at $\boldsymbol{r}$ at time t. For specified $\boldsymbol{r}$, one obtains

$$k_{q,i}(t) = \frac{\omega_{q,i}(t)}{c}, \quad k_{zq,i}(t) = \eta\frac{\omega_{q,i}(t)}{c} + \alpha_q \tag{30}$$

$$k_{\rho q,i}(t) = \sqrt{k_{q,i}^2(t) - k_{zq,i}^2(t)} = \frac{(-1)^i \alpha_q \rho}{c\sqrt{\tau^2 - \tau_0^2}} \tag{31}$$

where the radial wavenumber $k_{\rho q,i}(t)$ is calculated using (53). From (10), the corresponding local PFW propagation angles denoted for specified $\boldsymbol{r}$ by $\beta_{q,1}(t)$ and $\beta_{q,2}(t)$, respectively, become

$$\cos\beta_{q,i}(t) = k_{zq,i}(t)/k_{q,i}(t), \qquad i = 1, 2 \tag{32}$$

which implies via (28) that $\alpha_q/\omega_{q,i}(t)$ and, therefore, the angles $\beta_{q,i}(t) = \beta_i(t)$ do not depend on the FW index q. Using the

ray cone angle $\beta_0 = \cos^{-1}(\eta)$ in (10), (32) becomes equal to the *exact* expression in (18), which is defined directly in the TD. Thus, the asymptotic result obtained from the FD inversion turns out to be exact.

The asymptotic evaluation of the qth TD-FW integral in (26) is carried out via the formula [16, pp. 382]

$$\hat{A}_q^{\mathrm{FW}}(\boldsymbol{r}, t) \sim \sum_{i=1}^{2} F(\omega_{q,i}) \frac{\sqrt{2\pi} e^{-j\hat{\psi}(\omega_{q,i}(t))}}{\sqrt{j(d^2/d\omega^2)\hat{\psi}|_{\omega_{q,i}}}} U(\tau - \tau_0). \tag{33}$$

Substituting the values for $\hat{\psi}(\omega_{q,i}(t)) = \alpha_q z_i'(t)$ and $(d^2/d\omega^2)\hat{\psi}|_{\omega_{q,i}} = -\rho\alpha_q^2/(c^2 k_{\rho q,i}^3(t))$ we obtain

$$\hat{A}_q^{\mathrm{FW}}(\boldsymbol{r}, t) \sim \sum_{i=1}^{2} \hat{A}_{q,i}^{\mathrm{FW}}(\boldsymbol{r}, t) \tag{34}$$

in which $\hat{A}_{q,i}^{\mathrm{FW}}(\boldsymbol{r}, t)$ is the same as in (16). The unit step function $U(\tau - \tau_0) \equiv U(t - t_0)$ in the expressions for $\hat{A}_{q,i}^{\mathrm{FW}}(\boldsymbol{r}, t)$ occurs because the saddle point frequencies $\omega_{q,i}$ are real for $\tau > \tau_0$. For $\tau < \tau_0$, the $\omega_{q,i}$ are complex, do not lie on the integration path and therefore do not contribute dominantly to the saddle point approximation. Because the asymptotic and exact results agree, all interpretations relating to (16)–(23) apply as well. The fact that *all* TD-FW propagate simultaneously toward the observer is in accord with the instantaneous wavenumbers in (31). The asymptotic frequencies $\omega_{q,i}(t)$ are such that $|k_{zq,i}(t)| < |k_{q,i}(t)|$ whence, after turn-on $\tau > \tau_0$, $k_{\rho q,i}(t)$ in (31) is real. At the turn-on time $\tau = \tau_0$, we have $|k_{zq,i}(t_0)| = \infty$ and $|k_{\rho q,i}(t_0)| = \infty$. For $\tau \to \infty$ we have $\omega_{q,i}(t \to \infty) = \omega_{q,i}^{\mathrm{cutoff}}$ [see (29)]; thus the wavenumbers $|k_{zq,i}(t \to \infty)| = |k_{q,i}(t \to \infty)|$, with $|k_{\rho q,i}(t \to \infty)| = 0$, as in the text after (10). The solution in (34) can also be obtained by an *exact* inverse Fourier transform for any $q = 0, \pm 1, \pm 2, \ldots$ (see [19]).

In the nonradiating case, the solution of $(d\hat{\psi}/d\omega)|_{\omega_q} = 0$ is given by $\omega_{q,1}$ when $\eta > 0$ and by $\omega_{q,2}$ when $\eta < 0$, for all times $-\infty < \tau < \infty$, as shown in Appendix C. The saddle-point evaluation of (26) for the qth TD-FW is carried out via the expression in (33), with the summation and U-function omitted because $\omega_{q,i}(t)$ is now real for all $-\infty < \tau < \infty$, subject to the condition ($i = 1$, $\eta > 0$) and ($i = 2$, $\eta < 0$). Substituting the values $\hat{\psi}(\omega_{q,i}(t)) = \alpha_q z_i'(t)$ and $(d^2/d\omega^2)\hat{\psi}|_{\omega_{q,i}} = -\rho\alpha_q^2/(c^2 k_{\rho q,i}^3(t))$ we obtain for $\hat{A}_q^{\mathrm{FW}}(\boldsymbol{r}, t)$ the same value as in (24).

2) Group Velocity: The group velocity, which specifies the direction and propagation speed of the *energy flux* of the $\hat{A}_q^{\mathrm{FW}}$ wave field, is defined as $\boldsymbol{v}_{q,i}^{(g)} = (v_{\rho q,i}^{(g)};\ v_{zq,i}^{(g)})$, $v_{\rho q,i}^{(g)} = (\partial\omega(k_\rho, k_z)/\partial k_\rho)|_{q,i}$, $v_{zq,i}^{(g)} = (\partial\omega(k_\rho, k_z)/\partial k_z)|_{q,i}$, with $\omega(k_\rho, k_z) = c(k_\rho^2 + k_z^2)^{1/2}$. Thus, $\partial\omega/\partial k_\rho = ck_\rho/k$ and $\partial\omega/\partial k_z = ck_z/k$. Inserting the instantaneous wavenumbers from (30) and (31) and using the instantaneous propagation angle $\beta_i(t)$ in (32) yields

$$\boldsymbol{v}_{q,i}^{(g)} = c(\boldsymbol{i}_{\boldsymbol{\rho}} \sin\beta_i(t) + \boldsymbol{i}_{\boldsymbol{z}} \cos\beta_i(t)), \qquad i = 1, 2. \tag{35}$$

Since the angles $\beta_i(t)$ [see (18)] do not depend on the index q, the group velocity of each TD-FW does not depend on q. Thus, all instantaneous $\hat{A}_{q,i}^{\mathrm{FW}}(\boldsymbol{r}, t)$ fields propagate toward the observer along $\beta_i(t)$ with group velocity c. For schematization of the (space–time)-(wavenumber–frequency) interelations via space–time rays and dispersion surfaces (see [19]).

C. Analytic Signal Formulation

Inversion from the FD to the TD via the conventional Fourier transform pair in (1) often poses delicate problems because of the different roles played by the $\omega > 0$ and $\omega < 0$ frequency ranges. Such problems may be alleviated with analytic transforms which deal only with real positive frequencies $\omega > 0$ by extending the transient field into the complex TD. The analytic transform relations for a real space–time function $\hat{A}(\boldsymbol{r}, t)$ are (see [20], for example)

$$A(\boldsymbol{r}, \omega) = \int_{-\infty}^{\infty} \hat{A}(\boldsymbol{r}, t) e^{-j\omega t}\, dt \tag{36}$$

$$\overset{+}{A}(\boldsymbol{r}, t) = \frac{1}{\pi} \int_0^{\infty} A(\boldsymbol{r}, \omega) e^{j\omega t}\, d\omega, \qquad \Im mt \geq 0 \tag{37}$$

where the $^+$ symbol identifies the analytic continuation to complex time. As defined in (37), $\overset{+}{A}(\boldsymbol{r}, t)$ is analytic in the upper half of the complex t-plane, with its limit on the real-time axis given by

$$\overset{+}{A}(\boldsymbol{r}, t) = \hat{A}(\boldsymbol{r}, t) - j\boldsymbol{H}\{\hat{A}(\boldsymbol{r}, t)\}, \qquad t \text{ real} \tag{38}$$

where $\boldsymbol{H}$ stands for the Hilbert transform

$$\boldsymbol{H}\{\hat{A}(t)\} = \boldsymbol{P} \int_{-\infty}^{\infty} \frac{\hat{A}(t')}{\pi(t - t')}\, dt', \qquad t \text{ real} \tag{39}$$

with $\boldsymbol{P}$ denoting principal value integration. The real field $\hat{A}$ is, therefore, obtained by taking

$$\hat{A}(\boldsymbol{r}, t) = \Re e \overset{+}{A}(\boldsymbol{r}, t), \qquad t \text{ real.} \tag{40}$$

The results in (38)–(40) imply that the analytic (complex) TD can be accessed *directly* from the real TD through the definition

$$\overset{+}{A}(\boldsymbol{r}, t) = j \int_{-\infty}^{\infty} \frac{\hat{A}(\boldsymbol{r}, t')}{\pi(t - t')}\, dt', \qquad \Im mt > 0 \tag{41}$$

which avoids the FD entirely. For both formulations [in (37) with (36) and in (41), respectively], the real-time limit is recovered via (40).

The FW expansion for $\overset{+}{A}$ is given by $\overset{+}{A}(\boldsymbol{r}, t) = \sum_{q=-\infty}^{\infty} \overset{+}{A}_q^{\mathrm{FW}}(\boldsymbol{r}, t)$ in which the qth analytic $\overset{+}{A}_q^{\mathrm{FW}}(\boldsymbol{r}, t)$ field is the analytic transform (37) of the FD $A_q^{\mathrm{FW}}(\boldsymbol{r}, \omega)$ in (7). Using the synthesis of $A_q^{\mathrm{FW}}(\boldsymbol{r}, \omega)$ in (7) in terms of spatially distributed point-source radiators, interchanging the orders of integration (allowed because of the convergence introduced by $\Im mt > 0$) and performing the ω integration in closed form yields

$$\overset{+}{A}_q^{\mathrm{FW}}(\boldsymbol{r}, t) = \frac{j}{4\pi^2 d} \int_{-\infty}^{\infty} \frac{e^{-j\alpha_q z'}}{R(z') \left(t - \dfrac{\eta z'}{c} - \dfrac{R(z')}{c} \right)}\, dz'. \tag{42}$$

The correspondence between (42) and (12) is established via the analytic delta function $\overset{+}{\delta}(t) = j/(\pi t)$, $\Im m t > 0$, which follows from (41) on setting $\hat{A}(\boldsymbol{r}, t) = \delta(t)$. Note that the result in (42) could have been obtained directly in the TD via the analytic extension in (41) of $\hat{A}_q^{\mathrm{FW}}(\boldsymbol{r}, t)$ in (12).

The integral in (42) is now evaluated by deforming the integration path into the complex z'-plane and calculating the residues at the poles intercepted during the deformation. Since $R(z')$ [see (6)] has been defined in Appendix A such that $\Re e R(z') > 0$ on the top Riemann sheet of the complex z'-plane, the two branch cuts in accord with this condition extend as shown in Fig. 6. The integrand in (42) has poles defined via (13) and located at $z_i'(t)$ in (14). The loci of these poles vary with time t (which has been assigned a small positive imaginary part) as shown in Fig. 6. To understand and classify the pole singularities in the complex z'-plane, we again distinguish between the nondimensional parameter ranges $|\eta| < 1$ and $|\eta| > 1$ in (2). For the radiating case $|\eta| < 1$ the two solutions $z_1'(t)$ and $z_2'(t)$, given by the analytic version of (14), lie on the top Riemann sheet for $\tau > 0$, as shown in Fig. 6. For $\tau < 0$ the two solutions lie on the bottom Riemann sheet. If $q > 0$, i.e., $\alpha_q > 0$, the integrand in (42) converges exponentially in the lower half of the z'-plane, and the integration path can be deformed into the path C_L. The converse holds for $q < 0$. For $q > 0$, only the pole at $z_2'(t)$ is captured for $\tau > 0$ (i.e., $t > \eta z/c$). For $\tau < 0$ no poles are captured because they lie on the bottom sheet. Using the relation $R(z_i'(t)) = \tau c + \eta(z - z_i'(t))$ in (13), the $\overset{+}{A}_q^{\mathrm{FW}}(r, t)$ wavefield in (42) for $q > 0$ can be represented as the $z_2'(t)$-residue contribution plus the branch cut integral along C_L

$$\overset{+}{A}_q^{\mathrm{FW}}(r, t) = \frac{e^{-j\alpha_q z_2'(t)}}{2\pi d\sqrt{\tau^2 - \tau_0^2}}\, U(\tau) + \frac{j}{4\pi^2 d}\int_{C_L} \cdot \frac{e^{-j\alpha_q z'}}{R(z')\left(t - \dfrac{\eta z'}{c} - \dfrac{R(z')}{c}\right)}\, dz', \qquad q > 0. \tag{43}$$

The analytic TD FW includes one explicit term in closed form and also the integration around the branch cut. The term in closed form has the same form as the one in (16) (for $i = 2$) but differs by a factor of 2; in fact, the analytic signal is defined as twice the integral taken over the positive frequencies [see the factor 2 in the denominator in (1) and note that it is not present in (37)]. The closed-form term also differs by the argument of the unit step function. The real wavefield in the TD is obtained by taking the real part of the analytic signal $\overset{+}{A}_q^{\mathrm{FW}}(r, t)$. The term in closed form includes a precausal contribution because $U(\tau)$ is different from zero also for $0 < \tau < \tau_0$ (i.e., $\eta z/c < t < t_0$). The analytic FW is thus *noncausal* since the branch cut integral does not cancel the precausal closed-form term and, in fact, differs from zero also for $\tau < 0$ ($t < \eta z/c$). The analytic $(-q)$ FW (with $q > 0$), can be treated in a similar manner, with all analytic operations and contour deformations performed in the upper half plane because $\alpha_{-q} = -\alpha_q$. The contribution from the pole at $z_1'(t)$ now has to be accounted for in the deformation of the integration path around the upper branch cut C_U, leading

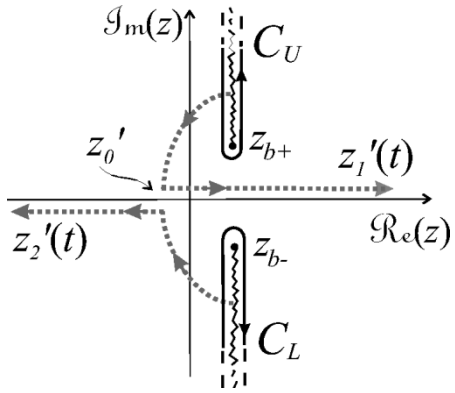

Fig. 6. Top Riemann sheet of the complex z'-plane, defined by $\Re e R(z') > 0$. Branch points are at $z_{b\pm} = z \pm j\rho$. The dotted loci track the roots $z_1'(t)$ and $z_2'(t)$ in (14). For $\eta z/c < t < t_0$, the two roots are complex conjugate; for $t > t_0 = \eta z/c + \tau_0$, the roots are real. The arrows on the loci point in the direction of increasing t. C_U and C_L are the integration paths in (43) and (44).

for $\overset{+}{A}_{-q}$ to the expression on the right side of (43), except that q, $z_2'(t)$, and C_L are replaced by $(-q)$, $z_1'(t)$ and C_U, respectively. The real fields $\overset{+}{A}_{\pm q}^{\mathrm{FW}}(\boldsymbol{r}, t)$ are obtained by taking the real parts of (43) and its counterpart for $-q$. It can be shown (see [19]) that the integral along C_U in $\overset{+}{A}_{-q}^{\mathrm{FW}}(r, t)$ is the complex conjugate of the integral along C_L in $\overset{+}{A}_q^{\mathrm{FW}}(\boldsymbol{r}, t)$. Thus

$$\begin{aligned}\hat{A}_{\pm q}^{\mathrm{FW}}(\boldsymbol{r}, t) &= \Re e \overset{+}{A}_{\pm q}^{\mathrm{FW}}(\boldsymbol{r}, t) \\ &= \Re e \frac{e^{\mp j\alpha_q z_i'(t)}}{2\pi d\sqrt{\tau^2 - \tau_0^2}}\, U(\tau) \pm \frac{1}{4\pi^2 d}\,\Im m \\ &\quad \cdot \int_{C_L} \frac{e^{-j\alpha_q z'}}{R(z')\left(t - \dfrac{\eta z'}{c} - \dfrac{R(z')}{c}\right)}\, dz'\end{aligned} \tag{44}$$

where $i = 1, 2$ for $\hat{A}_{-q}^{\mathrm{FW}}$ and $\hat{A}_{+q}^{\mathrm{FW}}$, respectively, with $q > 0$ ($\alpha_q > 0$). From the last expression in (44), it is noted that we can distinguish between the two $\pm q$ TD-FW's as defined here. Each is noncausal and, therefore, nonphysical. But when we sum the two real FW's $\hat{A}_{+q}^{\mathrm{FW}}(\boldsymbol{r}, t)$ and $\hat{A}_{-q}^{\mathrm{FW}}(\boldsymbol{r}, t)$ in (44), the two integral terms cancel, yielding the now *physical observable* wavefield, which is identical with that in (23)

$$\hat{A}_{obs}^{|q|\mathrm{FW}}(\boldsymbol{r}, t) \equiv \Re e \overset{+}{A}_{+q}^{\mathrm{FW}} + \Re e \overset{+}{A}_{-q}^{\mathrm{FW}} = (23). \tag{45}$$

The causal step function $U(\tau - \tau_0)$ [see (23)] follows from (44) because the noncausal closed-form terms vanish, when added, for $0 < \tau < \tau_0$. For τ in this interval, the square roots in (44) are complex conjugate $z_1'(t) = (z_2'(t))^*$ [see (14)] and, thus, $\Re e(j\exp(j\alpha_q z_1'(t))) + \Re e(j\exp(-j\alpha_q z_2'(t))) = 0$. The result in (45) for the observable FW_q wavefield, which was obtained via an entirely different parameterization of the problem than that leading to (23), thereby confirms the importance of $(+q)$, $(-q)$ pairing when defining physical causal Floquet wavefields. The analytic signal formulation in the complex z' plane gives fresh insights into the role played by complex source point (z') distributions which are known to generate beam-like fields with evanescent spectra [21].

D. The Cagniard–de Hoop Method

Finally, the TD-FW$_q$ potential field $\hat{A}_q^{\rm FW}$ is synthesized using the Cagniard–de Hoop method [13], [14], which applies conventionally to nondispersive wave processes. Because the TD-FW$_q$ is dispersive, we shall not apply the method in its standard form, which departs from an FD spectral integral representation that is manipulated into a Laplace integral for inversion by inspection. Instead, we express the FD field in terms of the *spatial* integration in (7) which is then converted into a standard Laplace transform. For simplicity, details are shown only for the radiating case $|\eta| < 1$. Introducing $s = j\omega$ into (7) yields

$$A_q^{\rm FW}(\boldsymbol{r}, -js) = \int_{-\infty}^{\infty} \frac{e^{-j\alpha_q z'}}{4\pi dR(z')}\, e^{-s/c[R(z')+\eta z']}\, dz'. \quad (46)$$

A Laplace transform is obtained by analytically continuing the imaginary parameter s to the positive real axis. First, note that (46) is defined for every $\Re es \geq 0$ since $[R(z') + \eta z'] > 0$ for large real z' (in fact, $R(z') \sim |z'|$ for large real z' and $[1 + \eta] > 0$ in the radiating case). The canonical mapping $[R(z') + \eta z']/c = t$, t real, onto the Laplace exponent $\exp(-st)$ then specifies the deformed integration path, on which the inversion is effected by inspection. This equation can be solved for z' to yield the two roots $z_1'(t)$ and $z_2'(t)$ in (14), which are tracked along the real axis in Fig. 6 for real $t > t_0$. [in Section V-C, it has already been established that the values $z_1'(t)$ and $z_2'(t)$ are complex for $t < t_0$, i.e., before the causal turn-on time t_0]. The index $i = 1, 2$ takes into account the multivaluedness of the z' solution that arises from the branch point at $t = t_0 = \eta z/c + \tau_0$ (or equivalently at $\tau = \tau_0 = \sqrt{1-\eta^2}\rho/c$) in (15). The paths $P_1 \equiv (z_0', \infty)$ and $P_2 \equiv (-\infty, z_0')$ in Fig. 6 are both mapped into the path (t_0, ∞) in the t plane (except for a minus sign for P_2) and the required contour deformations can be effected directly without crossing any singularities. Employing the mapping derivative

$$\left.\frac{dz'}{dt}\right|_{P_i} = \frac{-(-1)^i R(z_i')}{\sqrt{\tau^2 - \tau_0^2}} \qquad i = 1, 2 \qquad (47)$$

in (46) yields

$$A_q^{\rm FW}(\boldsymbol{r}, -js) = \sum_{i=1}^{2} \int_{t_0}^{\infty} \frac{e^{-j\alpha_q z_i'(t)}}{4\pi d\sqrt{\tau^2 - \tau_0^2}}\, e^{-st}\, dt \qquad (48)$$

which can be inverted by inspection. Since $U(t - t_0) = U(\tau - \tau_0)$, the result agrees with $\hat{A}_q^{\rm PFW}$ in (20). The transformation of the Kirchhoff integral in (7) into a directly invertible Laplace integral is another interesting outcome from this study. While applied here to the quasi-nondispersive FW, the transformation stays intact, of course, for the nondispersive $q = 0$ FW.

VI. Conclusion

In this paper, we have examined the simple canonical problem of radiation from an infinite periodic line array of dipoles excited impulsively with prescribed interelement time delay. This is the TD counterpart of a linearly phased line dipole array in the FD. By Poisson summation, the locally parameterized wavefield representation extending over the individual dipole radiators has been restructured collectively into a superposition of periodicity-induced FW. Exact closed-form expressions in the FD and TD have been derived as well as a variety of alternative spectral representations with different phenomenological interpretations. Coupled to relevant asymptotics, these studies have furnished detailed understanding of, and physical insight into, the impulse-source-excited TD behavior of FW dispersion. As enumerated in the introduction, we have been able to explain and clarify TD-FW behavior and anomalies from various perspectives both in the propagating (radiating) and nonpropagating (evanescent) regimes, generalizing previous studies [1]–[3] performed under more restrictive conditions. The $(+q)$ and $(-q)$ paired TD-FW wavefield observables are, to the best of our knowledge, new findings that are likely to have broad implications. The perspectives gained from this highly idealized canonical problem are expected to facilitate application to more realistic TD periodic array configurations, as demonstrated in [8], [9] for slot arrays. This will be the subject of future investigations, as is the TD generalization of the FD results for smooth line source arrays on slabs and truncated ground planes in [22], [23]. Especially promising is the analytic signal formulation which can address TD spectral (especially evanescent) subtleties in a fundamental manner.

Appendix A
Details Pertaining to (14)

We look for the z' solutions of (13) on the top Riemann sheet defined by $\Re eR(z') > 0$. Obtained by squaring, rearranging and solving the resulting quadratic equation, the solutions in (14) are also used in the analytic signal formulation of Section V-C. Therefore, we look, in addition, at the $\Im m(t \text{ or } \tau) \to 0^+$ limit of $z'(t)$ solutions. In order to determine under what conditions both $i = 1, 2$ solve the original equation (13), we insert (14) in (13), leading to

$$\frac{c}{1-\eta^2}\left(\tau + (-1)^i \eta\sqrt{\tau^2 - \tau_0^2}\right) = R(z_i'). \qquad (49)$$

For the radiating case $|\eta| < 1$, we have $1 + (-1)^i\eta > 0$, for $i = 1, 2$. For $\tau \gtrless 0$, one has $\Re e$ [left side of (49)] $\gtrless 0$, while the right side has $\Re e(R(z')) > 0$ on the top Riemann sheet of the z'-plane. Thus, there are no real $z_i'(t)$ solutions of (13) for $\tau < 0$, but two solutions $z_{1,2}'(t)$ on the top Riemann sheet for $\tau > 0$. For the nonradiating case $|\eta| > 1$, we have $1 - \eta^2 < 0$, $\tau_0 = -j|\tau_0|$, and (49) becomes

$$\frac{c}{1-\eta^2}\left(\tau + (-1)^i \eta\sqrt{\tau^2 + |\tau_0|^2}\right) = R(z_i'). \qquad (50)$$

The left and right sides are real for all real τ, and $\Re eR(z_i'(t)) > 0$. Since $|\tau| < \sqrt{\tau^2 + |\tau_0|^2}$, (50) implies that $\text{sgn}((-1)^i\eta) < 0$, therefore, the only solution of (13) on the top Riemann sheet is $z_1'(t)$ when $\eta > 0$ and $z_2'(t)$ when $\eta < 0$, for all τ.

APPENDIX B
ω-SYMMETRY PROPERTIES FOR FD-FWS

To ensure that a wave function $\hat{A}(\boldsymbol{r}, t)$ is real, its Fourier transform $A(\boldsymbol{r}, \omega)$ in (1) has to satisfy the well known property $A(\boldsymbol{r}, -\omega) = [A(\boldsymbol{r}, \omega)]^*$. We show here that the FD-FW $A_q^{\mathrm{FW}}(\boldsymbol{r}, \omega)$ in (7) does not satisfy this property but that $(+q)$ and $(-q)$ pairing does. Concerning $A_q^{\mathrm{FW}}(\boldsymbol{r}, \omega)$ given by the integral in (7), it is noted that $F(-\omega) \equiv \exp(-j(-\omega)R/c - jk_{zq}(-\omega)z) \neq [F(\omega)]^*$, since from (5), $k_{zq}(-\omega) \neq -k_{zq}(\omega)$. Thus, for $\alpha_q \neq 0$, $A_q^{\mathrm{FW}}(\boldsymbol{r}, -\omega) \neq [A_q^{\mathrm{FW}}(\boldsymbol{r}, \omega)]^*$. However, $k_{zq}(-\omega) = -k_{z,-q}(\omega)$, since $\alpha_{-q} = -\alpha_q$, thereby establishing that $A_q^{\mathrm{FW}}(\boldsymbol{r}, -\omega) = [A_{-q}^{\mathrm{FW}}(\boldsymbol{r}, \omega)]^*$. Accordingly, $A_q^{\mathrm{FW}}(\boldsymbol{r}, -\omega) + A_{-q}^{\mathrm{FW}}(\boldsymbol{r}, -\omega) = [A_q^{\mathrm{FW}}(\boldsymbol{r}, \omega) + A_{-q}^{\mathrm{FW}}(\boldsymbol{r}, \omega)]^*$. Q.E.D.

APPENDIX C
DETAILS PERTAINING TO (28)

Recalling (27), the saddle-point condition $d\hat{\psi}/d\omega = 0$ is

$$\eta z/c + \frac{k - \eta k_{zq}}{k_{\rho q}}\,\rho/c - t = 0. \tag{51}$$

Note that $\Re e(k_{\rho q}) \geq 0$ or ≤ 0 for $\omega > 0$ or < 0, respectively, in order to satisfy the radiation condition at $\rho = \infty$ for all ω. Squaring and rearranging yields, using (8)

$$\omega^2(1-\eta^2)A - 2\omega\eta\alpha_q cA - (\alpha_q c)^2(A + (\rho/c)^2) = 0 \tag{52}$$

with the two i-indexed solutions in (28). Here, $A = (\tau^2 - \tau_0^2)$. To sort out the correct combinations of $\pm\tau, \pm\alpha_q, \pm\eta$, we substitute (28) into the original equation (51) [recalling (5)] to obtain

$$\frac{(-1)^i\alpha_q}{c\sqrt{\tau^2 - \tau_0^2}} = \frac{k_{\rho q,i}}{\rho}, \qquad i = 1, 2. \tag{53}$$

For the radiating case $|\eta| < 1$, we have *real* values of $\omega_{q,i}$ in (28) only for $|\tau| > |\tau_0|$. Since, $(\tau^2 - \tau_0^2)^{1/2} < |\tau|$, the sign of $\omega_{q,i}$ depends on i through the sign of the second term inside the brackets in (28), i.e., $\mathrm{sgn}(\omega_{q,i}) = (-1)^i\mathrm{sgn}(\alpha_q\tau)$. Since $\mathrm{sgn}(\Re e k_{\rho q}) = \mathrm{sgn}(\omega)$, we have $\mathrm{sgn}(\Re e k_{\rho q,i}) = (-1)^i\mathrm{sgn}(\alpha_q\tau)$. Thus, both the left and right sides of (53) have the same sign for $\tau > \tau_0$ and opposite sign for $\tau < -\tau_0$, for $i = 1, 2$. This means that for $\tau > \tau_0$ both $\omega_{q,1}$ and $\omega_{q,2}$ are real solutions of (51) while neither of them is a solution for negative $\tau < -\tau_0$.

For the nonradiating case $|\eta| > 1, 1-\eta^2 < 0$, $(\tau^2 - \tau_0^2)^{1/2} = (\tau^2 + |\tau_0|^2)^{1/2} > |\tau|$, and thus in (28) $\mathrm{sgn}(\omega_{q,i}) = \mathrm{sgn}(-\alpha_q\eta)$. It follows that $\mathrm{sgn}(k_{\rho q,i}) = \mathrm{sgn}(-\alpha_q\eta)$ whence, to satisfy (53), $(-1)^i\mathrm{sgn}(\alpha_q) = \mathrm{sgn}(-\alpha_q\eta)$ or $(-1)^i = \mathrm{sgn}(-\eta)$. Thus, there is only one solution of (51): $\omega_{q,1}$ when $\eta > 0$ and $\omega_{q,2}$ when $\eta < 0$.

REFERENCES

[1] L. Carin and L. B. Felsen, "Time harmonic and transient scattering by finite periodic flat strip arrays: Hybrid (ray)–(Floquet mode)–(MoM) algorithm," *IEEE Trans. Antennas Propagat.*, vol. 41, pp. 412–421, Apr. 1993.

[2] L. B. Felsen and L. Carin, "Frequency and time domain Bragg-modulated acoustics for truncated periodic arrays," *J. Acoust. Soc. Amer.*, vol. 95, no. 2, pp. 638–649, Feb. 1994.

[3] ——, "Diffraction theory of frequency- and time-domain scattering by weakly aperiodic truncated thin-wire gratings," *J. Opt. Soc. Amer. A*, vol. 11, no. 4, pp. 1291–1306, Apr. 1994.

[4] F. Capolino, M. Albani, S. Maci, and L. B. Felsen, "Frequency domain Green's function for a planar periodic semi-infinite dipole array.—Part I: Truncated Floquet wave formulation," *IEEE Trans. Antennas Propagat.*, vol. 48, pp. 67–74, Jan. 2000.

[5] ——, "Frequency domain Green's function for a planar periodic semi-infinite dipole array.—Part II: Phenomenology of diffracted waves," *IEEE Trans. Antennas Propagat.*, vol. 48, pp. 75–85, Jan. 2000.

[6] F. Capolino, M. Albani, A. Neto, S. Maci, and L. B. Felsen, "Vertex-diffracted Floquet-waves at a corner array of dipoles," in *Int. Conf. Electromagn. Adv. Applicat. (ICEAA)*, Torino, Italy, Sept. 1997.

[7] F. Capolino, S. Maci, and L. B. Felsen, "Asymptotic high-frequency Green's function for a planar phased sectoral array of dipoles" (in invited paper), in *Ser. Spec. Issue 1998 URSI Int. Symp. Electromagn. Theory*, Thessaloniki, Greece, Mar,/Apr. 2000.

[8] A. Neto, S. Maci, G. Vecchi, and M. Sabbadini, "Truncated Floquet wave diffraction method for the full wave analysis of large phased arrays.—Part I: Basic principles and 2-D cases," *IEEE Trans. Antennas Propagat.*, vol. 48, pp. 594–600, Apr. 2000.

[9] ——, "Truncated Floquet wave diffraction method for the full wave analysis of large phased arrays.—Part II: Generalization to the 3-D cases," *IEEE Trans. Antennas Propagat.*, vol. 48, pp. 601–611, Apr. 2000.

[10] E. Heyman and L. B. Felsen, "Weakly dispersive spectral theory of transients,—Part I: Formulation and interpretation," *IEEE Trans. Antennas Propagat.*, vol. AP-35, pp. 80–86, Jan. 1987.

[11] ——, "Weakly dispersive spectral theory of transients,—Part II: Evaluation of the spectral integral," *IEEE Trans. Antennas Propagat.*, vol. AP-35, pp. 574–580, May 1987.

[12] E. Heyman, "Weakly dispersive spectral theory of transients—Part III: Applications," *IEEE Trans. Antennas Propagat.*, vol. AP-35, pp. 1258–1266, Nov. 1987.

[13] L. Cagniard, *Reflection and Refraction of Progressive Seismic Waves* (in translated from 1939 French monography by Flinn and Dix). New York: McGraw-Hill, 1962.

[14] A. T. de Hoop, "A modification of Cagniard's method for solving seismic pulse problems," *Appl. Sci. Res.*, vol. B8, pp. 349–356, 1960.

[15] A. Papoulis, *Systems and Transforms with Application in Optics*. Malabar, FL: Krieger, 1981.

[16] L. B. Felsen and N. Marcuvitz, *Radiation and Scattering of Waves*. Englewood Cliffs/Piscataway, NJ: Prentice-Hall/IEEE Press, 1973/1994.

[17] S. R. Deans, *The Radon Transform and Some of its Applications*. Malabar, FL: Krieger, 1993.

[18] D. Kralj, M. McClure, L. Carin, and L. B. Felsen, "Time-domain wave-oriented data processing of scattering by nonuniform truncated gratings," *J. Opt. Soc. Amer. A*, vol. 11, no. 10, pp. 2685–2694, Oct. 1994.

[19] L. B. Felsen and F. Capolino, "Time-domain Green's function for an infinite sequentially excited periodic line array of dipoles," Dept. Aerosp. Mech. Eng., Boston Univ., Boston, MA, Tech. Rep. AM-98-044, 1998.

[20] E. Heyman and L. B. Felsen, "Nondispersive closed form approximations for transient propagation and scattering of ray fields," *Wave Motion*, vol. 7, no. 1, pp. 335–358, 1985.

[21] ——, "Propagating pulsed beam solutions by complex source parameter substitution," *IEEE Trans. Antennas Propagat.*, vol. AP-34, pp. 1062–1065, Aug. 1986.

[22] L. Carin, L. B. Felsen, and T. T. Hsu, "High-frequency field excited by truncated arrays of nonuniform distributed filamentary scatterers on an infinite dielectric grounded slab: Parametrizing (leaky mode)–(floquet mode) interaction," *IEEE Trans. Antennas Propagat.*, vol. 44, pp. 1–11, Jan. 1996.

[23] F. Capolino, M. Albani, S. Maci, and R. Tiberio, "High-frequency analysis of an array of line sources on a truncated ground plane," *IEEE Trans. Antennas Propagat.*, vol. 46, pp. 570–578, Apr. 1998.

Leopold B. Felsen (S'47–M'54–SM'55–F'62–LF'90) was born in Munich, Germany, on May 7, 1924. He received the B.E.E., M.E.E, and D.E.E. degrees from the Polytechnic Institute of Brooklyn, Brooklyn, NY, in 1948, 1950, and 1952, respectively.

He emigrated to the United States in 1939 and served in the U.S. Army from 1943 to 1946. After 1952 he remained with the Polytechnic (now Polytechnic University), gaining the position of University Professor in 1978. From 1974 to 1978 he was Dean of Engineering. In 1994 he resigned from the full-time Polytechnic faculty and was granted the status of University Professor Emeritus. He is now Professor of Aerospace and Mechanical Engineering and Professor of Electrical and Computer Engineering at Boston University, Boston, MA. He is the author or coauthor of over 300 papers and of several books, including the classic *Radiation and Scattering of Waves* (Piscataway, NJ: IEEE Press, 1994). He is an associate editor of several professional journals and an editor of the *Wave Phenomena Series* (New York: Springer-Verlag). His research interests encompass wave propagation and diffraction in complex environments and in various disciplines, high-frequency asymptotic and short-pulse techniques, and phase-space methods with an emphasis on wave-oriented data processing and imaging.

Dr. Felsen is a member of Sigma Xi and a Fellow of the Optical Society of America and the Acoustical Society of America. He has held named Visiting Professorships and Fellowships at universities in the United States and abroad, including the Guggenheim in 1973 and the Humboldt Foundation Senior Scientist Award in 1981. In 1974 he was an IEEE/APS Distinguished Lecturer. He was awarded the Balthasar van der Pol Gold Medal from the International Union of Radio Science (URSI) in 1975, an honorary doctorate from the Technical University of Denmark in 1979, the IEEE Heinrich Hertz Gold Medal for 1991, the APS Distinguished Achievement Award for 1998, the IEEE Third Millenium Medal in 2000 (nomination by APS), three Distinguished Faculty Alumnus Awards from Polytechnic University, and an IEEE Centennial Medal in 1984. Also, awards have been bestowed on several papers authored or coauthored by him. In 1977 he was elected to the National Academy of Engineering. He has served as Vice Chairman and Chairman for both the United States and the International URSI Commission B.

Filippo Capolino (S'94–M'97) was born in Florence, Italy, in 1967. He obtained the Laurea degree (*cum laude*) in electronic engineering and the Ph.D. degree, both from the University of Florence, Italy, in 1993 and 1997, respectively.

From 1994 to 1999, he was a Teacher of antennas at the Diploma di Laurea, University of Siena, Italy, where he is currently a Research Associate. His research interests mainly concern theoretical and applied electromagnetics, with a focus on high-frequency methods for electromagnetic scattering.

Dr. Capolino received the MMET'94 Student Paper Competition Award in 1994, the Raj Mittra Travel Grant for Young Scientists in 1996, the "Barzilai" prize for the best paper at the National Italian Congress of Electromagnetism (XI RiNEm) in 1996, and the Young Scientist Award for participating at the URSI International Symposium on Electromagnetic Theory in 1998. In 1997, for six months, he was a Fulbright Research Visitor at the Department of Aerospace and Mechanical Engineering, Boston University, Boston, MA. From 1998 to 1999 he continued his research at Boston University under a Grant from the Italian National Council for Research (CNR).